View metadata, citation and similar papers at core.ac.uk
brought to you by CORE
provided by Archivio istituzionale della ricerca - Università di Palermo

Astronomy & Astrophysics manuscript no. nobold
October 25, 2013
© ESO 2013

arXiv:1310.6628v1 [astro-ph.HE] 24 Oct 2013

Discovery of periodic dips in the light curve of GX 13+1: the X-ray orbital ephemeris of the source

R. Iaria[1], T. Di Salvo[1], L. Burderi[2], A. Riggio[2], A. D'Aì[1], N. R. Robba[1]

[1] Dipartimento di Fisica e Chimica, Università di Palermo, via Archirafi 36 - 90123 Palermo, Italy
[2] Dipartimento di Fisica, Università degli Studi di Cagliari, SP Monserrato-Sestu, KM 0.7, Monserrato, 09042 Italy

October 25, 2013

ABSTRACT

Context. The bright low-mass X-ray binary (LMXB) GX 13+1 is one of the most peculiar Galactic binary systems. A periodicity of 24.27 d with a formal statistical error of 0.03 d was observed in its power spectrum density obtained with RXTE All Sky Monitor (ASM) data spanning 14 years.
Aims. Starting from a recent study, indicating GX 13+1 as a possible dipping source candidate, we systematically searched for periodic dips in the X-ray light curves of GX 13+1 from 1996 up to 2013 using RXTE/ASM, and MAXI data to determine for the first time the X-ray orbital ephemeris of GX 13+1.
Methods. We searched for a periodic signal in the ASM and MAXI light curves, finding a common periodicity of 24.53 d. We folded the 1.3-5 keV and 5-12.1 keV ASM light curves and the 2-4 and 4-10 keV MAXI light curves at the period of 24.53 d finding a periodic dip. To refine the value of the period we used the timing technique dividing the ASM light curve in eight intervals and the MAXI light curve in two intervals, obtaining four and two dip arrival times from the ASM and MAXI light curves, respectively.
Results. We improved the X-ray position of GX 13+1 using a recent Chandra observation. The new X-ray position is discrepant by $\sim 7''$ from the previous one, while it is compatible with the infrared and radio counterpart positions. We detected an X-ray dip, that is totally covered by the Chandra observation, in the light curve of GX 13+1 and showed, a-posteriori, that it is a periodic dip. We obtained seven dip arrival times from ASM, MAXI, and Chandra light curves. We calculated the delays of the detected dip arrival times with respect to the expected times for a 24.52 d periodicity. Fitting the delays with a linear function we find that the orbital period and the epoch of reference of GX 13+1 are 24.5274(2) days and 50,086.79(3) MJD, respectively. Adopting a quadratic ephemeris we do not improve the fit. The inferred orbital period derivative of $8(37)\times10^{-8}$ s/s, with the error at 68% confidence level, does not allow us to constrain the orbital evolution of the binary system.
Conclusions. We demonstrated the existence of periodic dips in the ASM and MAXI light curves estimating that the orbital period of GX 13+1 is 24.5274(2) d. GX 13+1 has the longest known orbital period for a Galactic neutron star LMXB powered by Roche lobe overflow.

Key words. stars: neutron – stars: individual (GX13+1) — X-rays: binaries — X-rays: stars – Astrometry and celestial mechanics: ephemerides

1. Introduction

GX 13+1 is a bright low-mass X-ray binary (LMXB); the detection of sporadic X-ray bursts (Fleischman 1985; Matsuba et al. 1995) suggests that the accreting compact object is a neutron star. Using infrared data Bandyopadhyay et al. (1999) estimated that the spectral type of the companion star is K5 III and the distance to the source is 7 ± 1 kpc. Ueda et al. (2001) detected, for the first time in a LMXB containing a neutron star, an absorption line, associated with Fe xxvi Kα, in the ASCA/SIS X-ray spectrum of GX 13+1, suggesting that the inclination angle of the system is relatively large. Using XMM/Epic-pn data Sidoli et al. (2002) found a more complex structure in the Fe-K region detecting absorption lines associated to Ca xx, Fe xxv Kα and Fe xxv Kβ, Fe xxvi Kα and Fe xxvi Kβ transitions. Ueda et al. (2004) studied the high-energy resolution spectrum of GX 13+1 taken by the Chandra high energy transmission grating spectrometer (HETGS) observing several absorption lines from highly ionised ions of Fe, Mn, Cr, Ca, Ar, S, Si, and Mg. The authors detected a significant blueshift of those lines suggesting that the ionised plasma has an outflow velocity of ~ 400 km s^{-1}. Furthermore, Ueda et al. (2004) inferred a mass outflow rate of $\dot{M} \geq 7\times10^{18}[(\Omega_{tot}/4\pi)/0.4]$ g s^{-1}, where Ω_{tot} is the total solid angle subtended by the plasma; this is comparable to the mass accretion rate in the inner part of the disk, 10^{18} g s^{-1}, estimated from the continuum spectrum.

Recently Díaz Trigo et al. (2012) analysed several XMM-Newton data sets of GX 13+1 fitting the continuum emission with a model consisting of disc-black body plus a black body component together with a Gaussian emission line at 6.55–6.7 keV. The authors also found that the continuum emission is absorbed by cold and photo-ionised material and constrained the inclination of GX13+1 to be between 60 and 80° because of the presence of strong absorption along the line of sight, obscuring up to 80% of the total emission in one observation, and the absence of eclipses. Although GX 13+1 is thought to be a high inclination angle system belonging to the Dipping source class of LMXBs the estimation of its orbital period is not simple because it is quite large.

Analysing the power spectrum of GX 13+1 obtained from RXTE All-Sky Monitor (ASM) data spanning 7 years Corbet (2003) detected a period of 24.07 ± 0.02 days. Corbet et al. (2010), using RXTE ASM data spanning 14 years, estimated a

Send offprint requests to: R. Iaria, e-mail: rosario.iaria@unipa.it

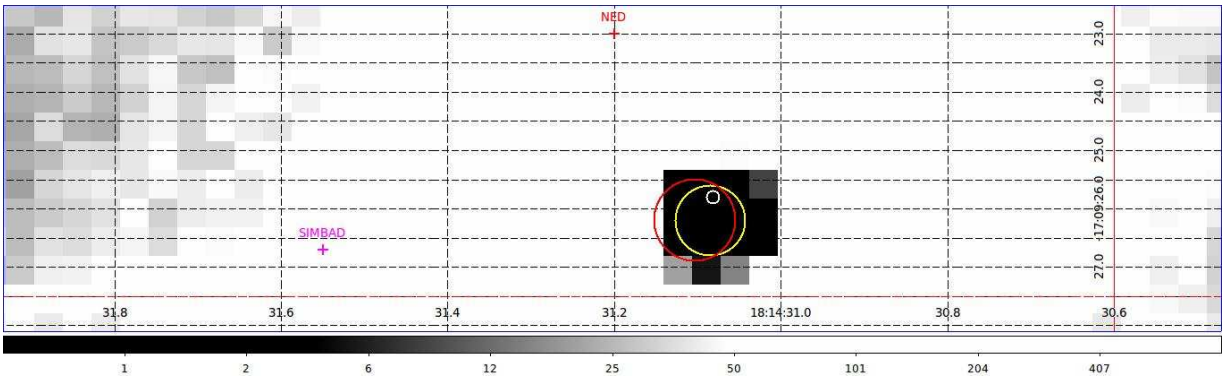

Fig. 1. Chandra/HETGS image of GX 13+1 obtained from the reprocessed level2-event file. The image is a detail close to the X-ray position. The grey scale represents the number of photons for each pixel integrated along the whole duration of the observation. Close to the zero-order position the number of events is almost zero because of the strong pile-up. The yellow circle centred at RA= 273°.62952 and DEC= −17°.157275 indicates the updated position of GX 13+1 reported in this paper, the red and white circles indicate the error boxes of the infrared and radio counterparts of GX 13+1. The magenta and the red crosses indicate the previous X-ray position of GX 13+1 in the SIMBAD and NED catalogue, respectively.

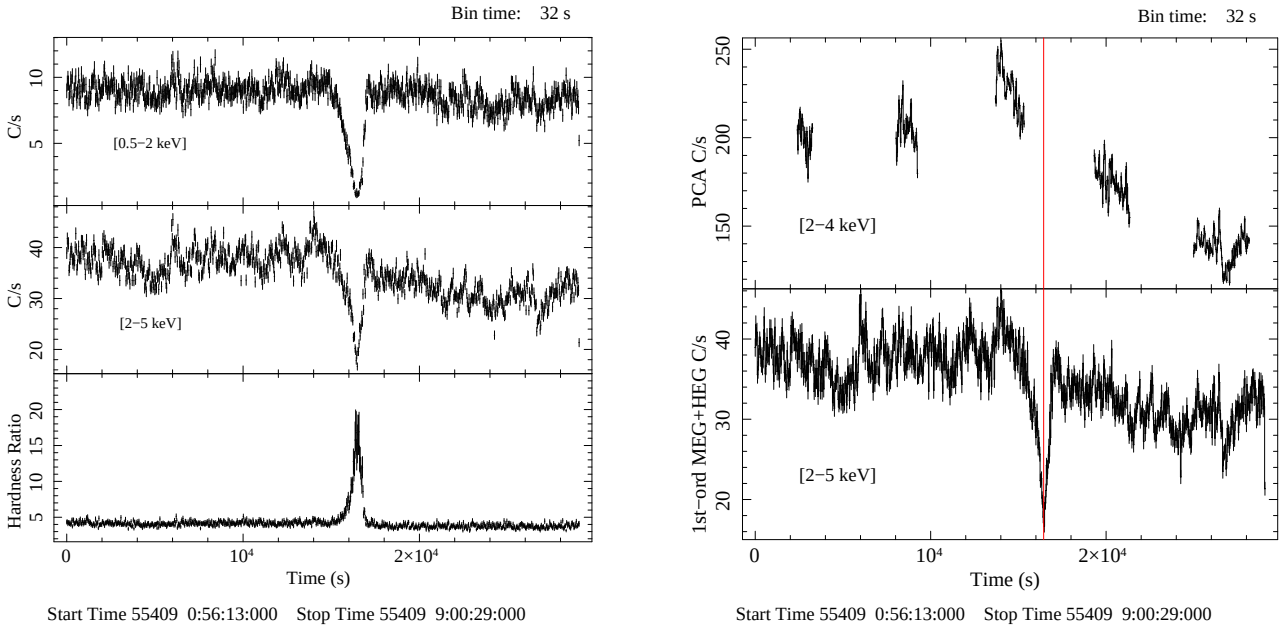

Fig. 2. Left Panel: Chandra light curve of GX 13+1 between 55,409.03 and 55,409.37 MJD. Summed first-order MEG and HEG light curves in the 0.5-2 keV energy band (top), in the 2-5 keV energy band (middle), and the corresponding hardness ratio (bottom) are shown. The bin time is 32 s. Right Panel: background subtracted RXTE/PCA light curve of GX 13+1 in the 2-4 keV energy band (top) and Chandra light curve of GX 13+1 in the 2-5 keV energy band (bottom). The solid vertical line indicates the estimated dip arrival time. The bin time is 32 s.

period of 24.27 ± 0.03 days. If the periodicity of 24 days is the orbital period of the binary system then GX 13+1 has the longest known orbital period for a Galactic neutron star LMXB; however, Corbet et al. (2010) noted that the periodic signal observed in the power spectrum is not strictly coherent and suggested that it might be caused by a structure that is not completely phase-locked with the orbital period. Corbet et al. (2010) proposed that the X-ray variability may be caused by an unresolved dipping modulation.

In this work we report the first ephemeris of GX 13+1 with an accuracy of the orbital period by a factor one hundred larger than the previous value proposed by Corbet et al. (2010). The periodic dips are clearly observed in the RXTE/ASM light curve spanning almost 16 years, in the MAXI light curve spanning 4 years, and during a recent Chandra/HETGS observation.

2. Observations

2.1. Chandra

Chandra observed GX 13+1 nine times from 2000 to 2011. The corresponding obsids are 950 (see Smith, Edgar & Shafer 2002), 2708 (see Ueda et al. 2001), 6093 (see Smith 2008), 11814, 11815, 11816, 11817, 11818, and 13197. We searched for the presence of dips in these light curves, finding one clear dip signature in the obsid 11814. It was taken on 2010 August

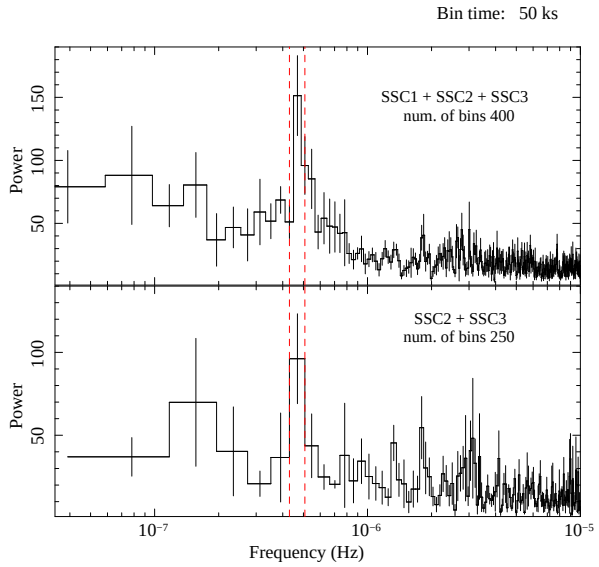

Fig. 3. Power spectrum densities of the 1.3-12.1 keV ASM light curve including all the SSCs (top panel) and only SSC2 and SSC3 (bottom panel). We adopted a bin time of 50 ks for both the light curves and a number of bins of 400 and 250, respectively. A periodic signal is evident in both the light curves and corresponds to a period between 22.78 and 26.92 d that are indicated with the vertical dashed-red lines.

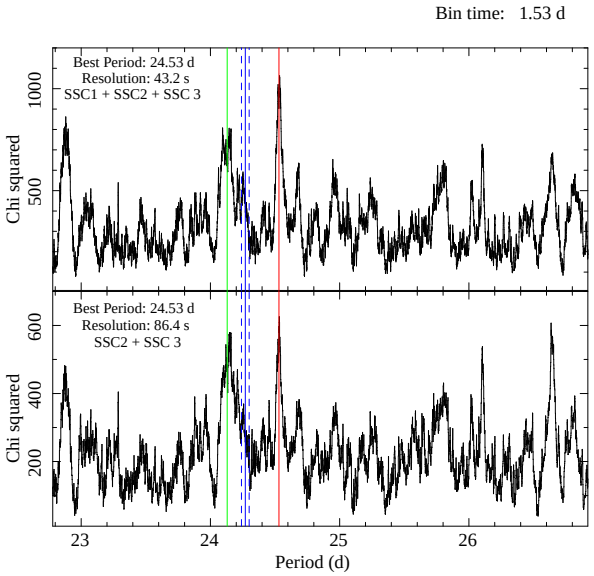

Fig. 4. Folding search of periodicities between 22.78 and 26.92 d in the ASM light curve including all the SSCs (top panel) and including only SSC 2 and 3 (bottom panel), respectively. We adopted 16 phase-bins per period for the trial folded light curves and a resolution in the period search of 43.2 s (top panel) and 86.4 s (bottom panel). The maximum of χ^2 is observed at 24.53 d (red vertical line) in both the curves. The vertical green-solid line indicates a possible periodicity at 24.12 d. The vertical blue-solid and blue-dashed lines indicate the period of 24.27 ± 0.03 d suggested by Corbet et al. (2010).

1 00:31:31 UT for an exposure time of 29 ks and performed in Timed Graded mode using the High Energy Transmission Grating Spectrometer (HETGS). We reprocessed the data and used the level2-event file to update the X-ray coordinates of GX 13+1. Because the zero-order X-ray image is strongly piled-up, the new coordinates were determined by fitting the intersection of the grating arms positions with the source readout streak (similarly to the pipeline adopted by Iaria et al. (2006) and Iaria et al. (2007)). The updated X-ray coordinates of the source are RA= 273°.62952 and DEC= −17°.157275 (referred to J2000.0) with an associated error of 0″.6, that is the overall 90% uncertainty circle of the Chandra X-ray absolute positional accuracy[1]. We obtained very similar values using the Chandra script *tg_findzo*. The new X-ray position is at 6″.7 from that reported in the SIMBAD catalogue, while it is compatible with the infrared (Garcia et al. 1992) and radio (Grindlay & Seaquist 1986) counterpart positions. We show in Fig. 1 the new estimated position with the corresponding error marked by a yellow circle; the red and white circles indicate the error boxes of the infrared and radio counterpart positions of GX 13+1. The magenta and red crosses indicate the previous X-ray position of GX 13+1 in the SIMBAD and NED catalogue, respectively.

We barycentred the level-2 event file with respect to the new X-ray coordinates using the tool *axbary* in the CIAO package, and, finally, extracted the light curves in the 0.5-2 keV and 2-5 keV energy bands from the level-2 event file using the Chandra tool *dmextract* adding the first-order MEG and HEG and adopting a bin time of 32 s. The light curves and the corresponding hardness ratio (HR) are shown in Fig. 2 (left panel).

The large increase of the HR around 16,000 s from the beginning of the observation (see left-bottom panel of Fig. 2) suggests a large photoelectric absorption; the 0.5-2 keV count rate decreases more rapidly than the 2-5 keV count rate, that is typical of a dip phenomenon. To estimate the arrival time of the dip we fitted the HR data between 16,000 and 16,900 s, corresponding to the maximum of the hardness ratio, with a constant plus a Gaussian profile assuming the centre of the Gaussian to be the arrival time of the dip. We assumed as a 1-sigma uncertainty to this measure the statistical error derived from the best-fitting centre of the Gaussian. The observation was taken between 55,409.03 and 55,409.37 MJD. We estimated that the minimum of the dip occurs at 55,409.22935(11) MJD.

Simultaneously the PCA on board of *Rossi-XTE* (RXTE) observed GX 13+1 on 2010 August 1 from 01:29:03.56 UT to 08:38:55.56 UT (observations P95338-01-01-04, P95338-01-01-03, P95338-01-01-02, P95338-01-01-01, and P95338-01-01-05). We show the RXTE/PCA background-subtracted light curve of GX 13+1, obtained from the standard products in the 2-4 keV energy range, in the right-top panel of Fig. 2. For sake of clarity we also show in the right-bottom panel of Fig. 2 the summed first-order MEG and HEG light curve in the 2-5 keV energy range. Unfortunately, the RXTE/PCA observation does not cover the dip observed by Chandra. The dip arrival time is indicated with the solid vertical line in Fig. 2 (right panels).

2.2. RXTE/ASM and MAXI

With the aim to find periodic dips, we analysed the light curve of GX 13+1 taken by the ASM on board RXTE; the light curve spans around 16 years from 50,088.21 to 55,865.44 MJD. The ASM consists of three Scanning Shadow Cameras (SSCs)

[1] See `http://cxc.harvard.edu/cal/ASPECT/celmon/` for more details

mounted on a rotating drive assembly. First of all, we barycentred the ASM light curve of GX 13+1 with respect to the new X-ray coordinates using the tool *faxbary*. We extracted the 1.3-12 keV ASM light curve from each SSC. The SSC 1 light curve shows a slightly decline of the flux in agreement with what is reported by Corbet et al. (2010). Using the ftools *powspec* in the XRONOS package we produced two power spectrum densities (PSDs). The first PSD was obtained from the ASM light curve including all the SSC events (hereafter SSC123 light curve) and the second one including only the SSC2 and SSC3 events (hereafter SSC23 light curve). We used a bin time of 50 ks for both the PSDs and a number of bins of 400 and 250 for the SSC123 and SSC23 light curve, respectively. A periodic signal between 22.78 and 26.92 d (indicated in frequency with the vertical red-dashed lines in Fig. 3) is evident in both the PSDs. We explored the period-window between 22.78 and 26.92 d using the ftools *efsearch* in the XRONOS package for both the light curves. We adopted 16 phase-bins per period (that is a bin time close to 1.53 d) for the trial folded light curves and a resolution of the period search of 43.2 s and 86.4 s for the SSC123 and SSC23 light curve, respectively. We observe the largest peak of χ^2 close to 24.53 d for both the light curves (vertical red line in Fig. 4), a smaller peak is observed at 24.12 d that is indicated in Fig. 4 with a vertical green-solid line. We also note that the periodicity of 24.27 ± 0.03 d (vertical blue-solid and blue-dashed lines in Fig. 4) suggested by Corbet et al. (2010) is not significantly detected in our search. Since we obtained the same periodic signals independently of the inclusion or exclusion of the SSC1 events, we conclude that the decline of the flux in the SSC1 does not affect our analysis. We, therefore, used, in the following, the ASM light curves including all the SSCs to obtain the largest available statistics.

We searched for periodic signals also in the one-orbit 2-10 keV light curve of GX 13+1 taken by the Monitor of All-sky X-ray Image (MAXI) on board of the International Space Station (ISS) (see Matsuoka et al. 2009). The light curve spans about 4 years. Adopting the new X-ray coordinates of GX 13+1, we barycentred the light curve with respect to the centre of mass of the solar system using the ftool *earth2sun*. Using the ftool *efsearch* we searched for periodicities between 22.78 and 26.92 d adopting 16 phase-bins per period in the trial folded light curves and a resolution of the period search of 86.4 s. We found three peaks of the χ^2 which were fitted with Gaussian profiles; the centres of the three Gaussian profiles are close to 24 d, 24.53 d and 25.6 d (see Fig. 5). The periodicity at 24.53 d (red-solid line in Fig. 5) is the same found analysing the ASM light curve. The periodic signal at 24 d (green-solid line in Fig. 5) is an instrumental signal due to a not appropriately subtraction of the background from the data collected by the 1550V cameras. The 1550V cameras collect events from the region of sky containing GX 13+1 for 24 days with respect to the total period of precession of the ISS (i.e. 70 days) and it leaves an excess of counts which varies in 24 days (Tatehiro Mihara, MAXI team; private communication). The periodicity at 25.6 d (green-dashed line in Fig. 5) is similar to the period of 25.8 ± 0.03 d observed in the K-band light curve of GX 13+1 (Corbet et al. 2010). A similar but less significant periodic signal seems to be present in the ASM light curve at ∼25.8 d. We plot the 25.6 d folded 2-4 and 4-10 keV MAXI light curves and the corresponding HR in Fig. 6 using as epoch 55,044.77 MJD and 100 phase-bins per period. A clear sinusoidal modulation with a period of 25.6 d is present in the HR. However, because we are interested in the presence of possible periodic dips in the ASM and MAXI light curves we will not discuss further this periodic signal. Finally, the vertical blue-dashed and blue-solid lines indicates the period of 24.27 ± 0.03 d suggested by Corbet et al. (2010), that is not significantly detected in our search.

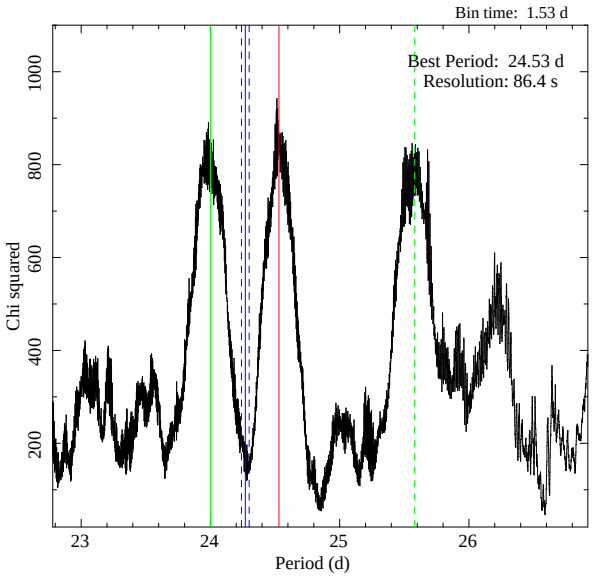

Fig. 5. Folding search of periodicities in the 2-10 keV MAXI light curve between 22.78 and 26.92 d. We adopted 16 phase-bins per period for the trial folded light curves and a resolution of period search of 0.001 d. The vertical blue-solid and blue-dashed lines correspond to the period 24.27 ± 0.03 d suggested by Corbet et al. (2010). Three peaks of χ^2 are detected: at 24.53 d (vertical red line), at 25.6 d (vertical green-dashed line), and at 24 d (vertical green-solid line). The latter period is an instrumental artifact (see text).

We folded the ASM light curves in the 1.3-5 keV and 5-12.1 keV using as folding period 24.12 d, 24.53 d, and 24.27 d, respectively, obtaining three folded light curves for each adopted energy band. The ASM folded light curves and the corresponding HRs are shown in Fig. 7; the folded light curves are obtained using 128 phase bins per period. The 24.53 d folded light curves highlight the presence of a dip in the ASM light curve of GX 13+1. The 1.3-5 keV and 5-12.1 keV light curves show a decrease of the count rate from 12.2 to 10.1 c/s and from 8.9 to 8.3 c/s, respectively, close to phase 0 (see Fig. 7, right panel). At the same phase the HR increases from 0.75 to 0.84. This suggests that the equivalent hydrogen column density associated to the local neutral (or partially ionised) matter increases close to phase 0 causing a reduction of the count rare at low energies and, consequently, an increase in the HR. A similar modulation is not observed at 24.12 d (see Fig. 7, left panels) and it is less significant using as folding period 24.27 d (see Fig. 7, centre panels). We show the 2-4 and 4-10 keV MAXI folded light curves and the corresponding HRs in Fig. 8. We folded them using the periods of 24.12, 24.27 and 24.53 d and adopting 128 phase-bins per period. Also in this case we found that a periodic dip is present close to phase 0 in the 24.53 d folded MAXI light curves (Fig. 8, right panels); the dip is absent in the 24.12 and 24.27 d folded MAXI light curves. During the dip the MAXI count rate per cm^{-2} decreases from 0.54 to 0.46 and from 0.49 to 0.46 in the 2-4 and 4-10 keV folded light curves, respectively, the HR increases from 0.92 to 1.01 We conclude that a periodic signal at a period of 24.53 d is present both in the 1.3-12.1 keV ASM

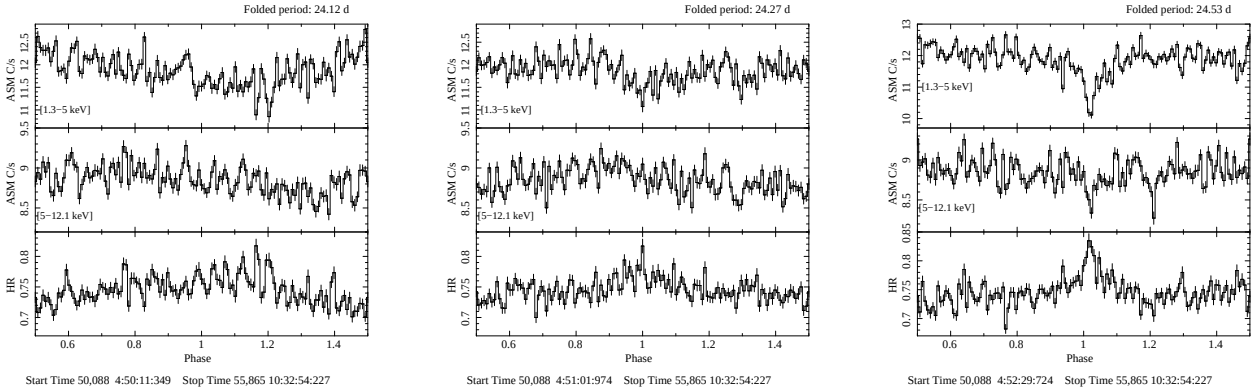

Fig. 7. RXTE/ASM folded light curves of GX 13+1 using the folding period 24.12 d (left panel), 24.27 d (middle panel), and 24.53 d (right panel). We show the folded light curves in the 1.3-5 keV (upper panels) and 5-12.1 keV (middle panels) energy band, and the corresponding hardness ratios (bottom panels) for each folding period. The folded light curves are obtained using 128 phase-bins per period.

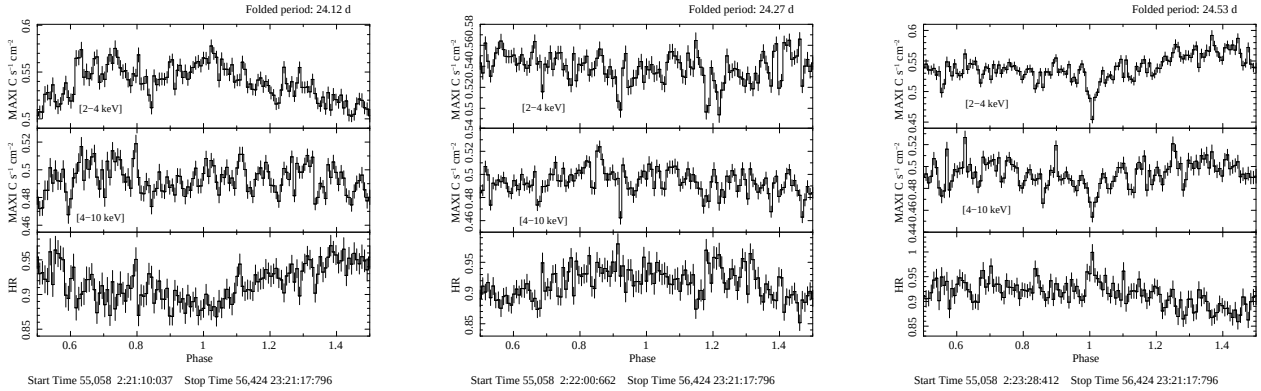

Fig. 8. MAXI folded light curves of GX 13+1 using as folding period 24.12 d (left panel), 24.27 d (middle panel), and 24.53 d (right panel). We show the folded light curves in the 2-4 keV and 4-10 keV energy band and the corresponding hardness ratios for each folding period. The folded light curves are obtained using 128 phase-bins per period.

and 2-10 keV MAXI light curve; furthermore, the 24.53 d folded light curves highlights the presence of a periodic dip.

2.3. EXOSAT

Encouraged by these results, we looked for historical observations of GX 13+1, in order to find periodic dips in pointed observations, starting with EXOSAT. We used the Medium energy (ME) light curves in the NASA archive[2] The ME instrument on board EXOSAT observed GX 13+1 on 1983 Sep. 22 (seq. number 192), 1985 Apr. 1 (seq. number 1488) and 1985 May 2 (seq. number 1549). We analysed the corresponding 1-3.8 and 3.8-8 keV light curves and the corresponding HR; the light curves at the two different energy bands and the HRs are shown in Fig. 9 and 10.

We note that the light curves corresponding to the observation taken on 1983 Sep. 22 (Fig. 9) show a decrease of count rate at around 3,000 s from the start time in both the energy bands and the corresponding HR changes slightly going from 1.1 to 1.2. The light curves corresponding to the observation taken on 1985 May 2 (see Fig. 10) show a long-term modulation of the hardness ratio that it is difficult to ascribe to the presence of a dip. During the first 15 ks from the beginning of the observation the HR increases from 1.1 to 1.4; at 17.5 ks from the start time it rapidly increases from 1.1 to 1.3, in the last part of the observation it is quite constant at 1.15. Although it is evident a change of the HR in the EXOSAT observation taken in 1985 we are not able to ascribe this behaviour to a dip. For this reason in our analysis we will not use the EXOSAT observations.

2.4. XMM/RGS

XMM-Newton observed GX 13+1 nine times; a complete analysis of the RGS and Epic-pn light curves and spectra of the source has been recently reported by Díaz Trigo et al. (2012). The most significant detection of a dip is during the observation ID 0505480501 taken on 2008 March 25. However, the dip was observed only partially by the RGS because it occurred at the beginning of the observation while the EPIC-pn was still off. The start and stop times of the RGS observation are 54,550.97 and 54,551.12 MJD, respectively. We show the background-subtracted light curves of the summed 1st-order RGS1 and RGS2 data in the 0.3-1.5 keV (Fig. 11, upper panel) and 1.5-2.5 keV (Fig. 11, middle panel) energy band. The corresponding HR is shown in the lower panel of Fig. 11. The HR is

[2] The standard filtering of the ME light curves is shown at `heasarc.gsfc.nasa.gov/W3Browse/exosat/me.html`

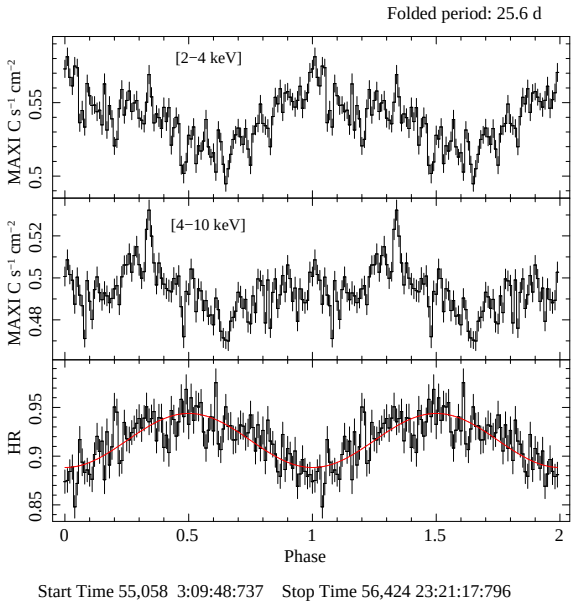

Fig. 6. 25.6 d folded 2-4 keV and 4-10 keV MAXI light curves (upper and middle panel, respectively). The HR is shown in the bottom panel. We adopted 100 phase-bins per period and Epoch 55,044.77 MJD. The HR shows an evident sinusoidal modulation (red curve in bottom panel) at the folded period.

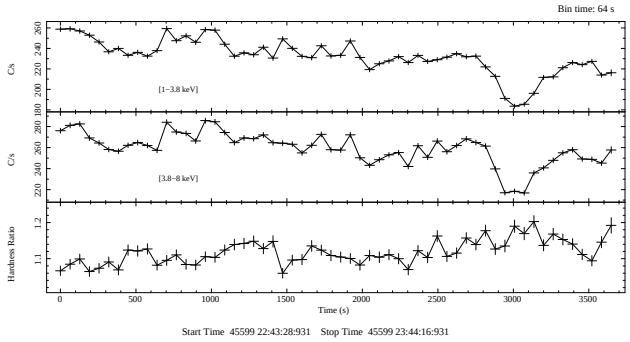

Fig. 9. EXOSAT/ME observation of GX 13+1 between 45,599.95 and 45,599.99 MJD. Light curves in the 1-3.8 keV (top panel), in the 3.8-8 keV (middle panel) energy band, and the corresponding hardness ratio (bottom panel) are shown. The bin time is 64 s.

the hardest (about 7) during the first 1,000 s of the observation, then drops to a value of 4, suggesting that the decrease of the RGS count rate at the beginning of the observation is associated with a dipping phenomenon.

We do not have a complete coverage of the dip and are not able to give a precise estimate of the dip arrival time. To get more information on this dip, we looked for it in the 1.3-5 keV RXTE/ASM light curve. We show the RXTE/ASM light curve between 54,545 and 54,555 MJD in Fig. 12; the start and stop times of the RGS observation are indicated with the red-dashed vertical lines. The ASM light curve of GX 13+1 shows that the RGSs observed only the end of the dip. We will not take into account this dip for our analysis, because we were not able to estimate exactly its arrival time. However, we will comment a-posteriori our results comparing them with the ASM light curve shown in Fig. 12.

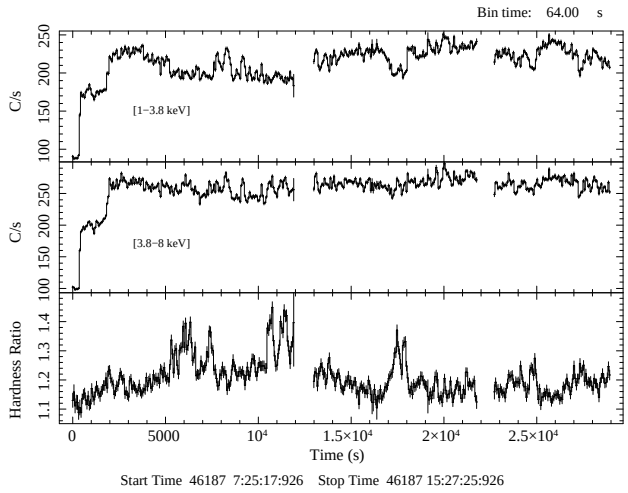

Fig. 10. EXOSAT/ME observation of GX 13+1 between 46,187.31 and 46,187.64 MJD. Light curves in the 1-3.8 keV (top panel), in the 3.8-8 keV (middle panel) energy band, and the corresponding hardness ratio (bottom panel) are shown . The bin time is 64 s.

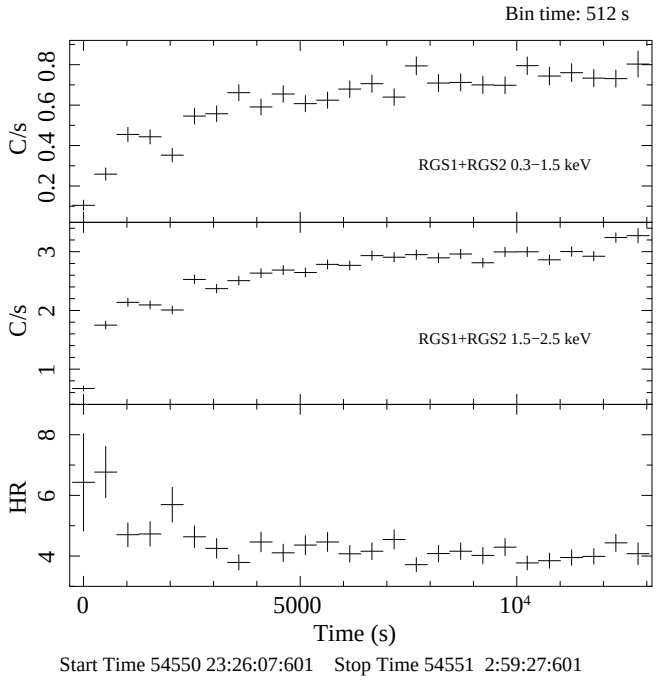

Fig. 11. RGS light curves during the observation ID 0505480501, between 54,550.97 and 54,551.12 MJD. Upper panel: 0.3-1.5 keV RGS light curve. Middle Panel: 1.5-2.5 keV RGS light curve. Lower panel: the corresponding HR. The bin time is 512 s.

3. Ephemeris of GX 13+1

To estimate with the best accuracy the period of GX 13+1 we used a timing technique (see e.g. Iaria et al. (2011) and references therein, for an example of the application of timing techniques to improve orbital ephemeris). In order to obtain several dip arrival times we divided the 1.3-5 keV and 5-12.1 keV ASM light curves in eight intervals. The corresponding temporal windows of each of the eight light curves cover about 29 cycles ($\sim$ 714 days). For each interval, the soft and hard

Table 1. Journal of the X-ray dip arrival times of GX 13+1

Interval	Tstart (MJD;TDB)	Tstop (MJD;TDB)	Dip Time (MJD;TDB)	Cycle	Delay (days)	Satellite
1	50,088.19	50,804.79	50,454.66(8)	15	0.86(8)	RXTE/ASM
4	52,290.96	52,983.03	52,637.61(6)	104	1.53(6)	RXTE/ASM
7	54,467.60	55,182.58	54,844.97(6)	194	2.09(6)	RXTE/ASM
			55,409.22935(11)	217	2.38935(11)	Chandra/HETGS
1	55,058.09	55,741.47	55,409.30(15)	217	2.45(15)	MAXI
2	55,741.59	56,424.97	56,096.04(6)	245	2.67(6)	MAXI

Note — Epoch of reference 50, 086 MJD, orbital period 24.52 days.

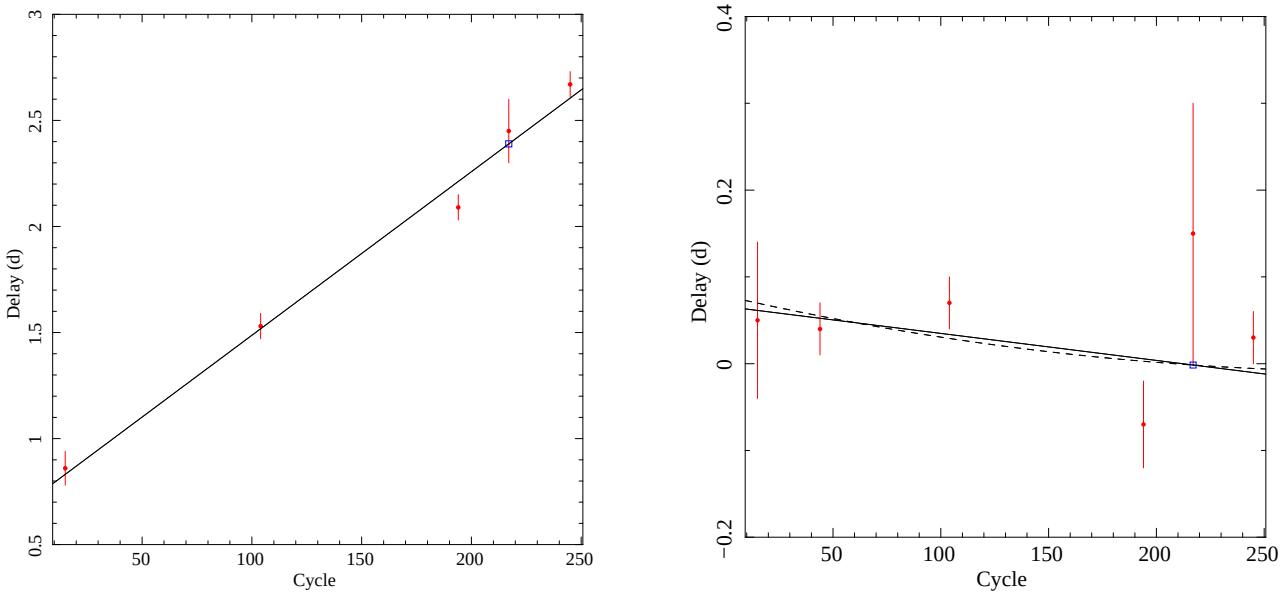

Fig. 15. Delays in units of days of the dip arrival times plotted versus the corresponding cycle number; the Chandra point is indicated with a blue open square. Left panel: trial period of 24.52 d and epoch 50,086 MJD; the solid line represents the linear ephemeris shown in eq. 1. Right panel: trial period of 24.5277 d and epoch 50,086.72 MJD. The solid line and the dashed curve indicate the linear ephemeris shown in Eq. 2 and the quadratic ephemeris of Eq. 3, respectively.

Table 2. Journal of the refined X-ray dip arrival times of GX 13+1

Interval	Tstart (MJD;TDB)	Tstop (MJD;TDB)	Dip Time (MJD;TDB)	Cycle	Delay (days)	Satellite
1	50,088.19	50,804.79	50,454.69(9)	15	0.05(9)	RXTE/ASM
2	50,816.23	51,506.13	51,165.98(3)	44	0.04(3)	RXTE/ASM
4	52,290.96	52,983.03	52,637.67(3)	104	0.07(3)	RXTE/ASM
7	54,467.60	55,182.58	54,845.16(5)	194	-0.07(5)	RXTE/ASM
			55,409.22935(11)	217	-0.00157(11)	Chandra/HETGS
1	55,058.09	55,741.47	55,409.38(15)	217	0.15(15)	MAXI
2	55,741.59	56,424.97	56,096.03(3)	245	0.03(3)	MAXI

Note — Epoch of reference 50, 086.72 MJD, orbital period 24.5277 days.

light curves were folded adopting an arbitrary folding period of 24.52 d (close to 24.53 d observed in the ASM and MAXI light curves), an arbitrary reference time of 50,086 MJD, and, finally, 150 phase-bins per period. The presence of a periodic dip in the folded light curves was significantly detected only in intervals 1, 4, and 7 (Fig. 13), the start and stop times of these intervals are shown in Tab. 1. To estimate the dip arrival times we fitted the 1.3-5 keV folded light curves with a model consisting of a constant plus a sinusoidal function, with the period kept fixed to 1 (that is 24.52 d), adding a Gaussian component with a negative normalisation to fit the dip shape and assuming the centroid of the Gaussian component as the dip arrival times. We took care to fit only the dip in the 1.3-5 keV folded light curve showing an evident increase of the HR [5 – 12.1keV]/[1.3 – 5keV].

Adopting the same procedure we divided the 2-4 keV MAXI light curve into two intervals, the corresponding temporal windows of each of the two MAXI light curves cover about 28 cycles

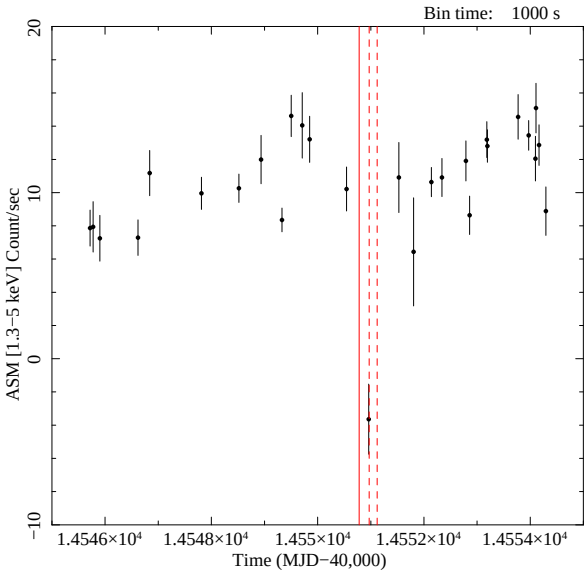

Fig. 12. RXTE/ASM light curve of GX 13+1in the 1.3-5 keV energy band between 54,545 and 54,555 MJD. The bin time is 1000 s. The dotted vertical lines indicate the start and stop times of the RGS observation. The solid vertical line indicates the expected dip arrival time (i.e. 54,550.78 MJD) adopting the ephemeris of eq. 2 (see the text).

(∼ 680 days). We show the MAXI folded light curves in Fig. 14 and report the journal of the X-ray dip arrival times in Table 1.

This analysis allows us to obtain five dip arrival times from the ASM and MAXI light curves. Note that, in order to increase the statistics in the ASM and MAXI light curves, we selected large temporal windows, covering 29 and 28 cycles in the RXTE/ASM and MAXI light curves, respectively. We adopted as Epoch of reference the arbitrary value of 50,086 MJD and calculated the delays of the dip arrival times with respect to those predicted by the trial folding period of 24.52 d. We assigned to each temporal window the cycle number corresponding to the half time of the window. We, initially, fitted the delays vs orbital cycle with a linear function f and took into account only the errors associated to the dip arrival times (hereafter Δy)

obtaining a first estimation of the corrections to the epoch of reference and orbital period. Since each temporal window contains a large number of cycles we took into account the uncertainty associated to this large number combining Δy with the error associated to the cycles (hereafter Δx) using the relation $(\Delta_{tot})^2 = (\Delta y)^2 + (\partial f/\partial x\, \Delta x)^2$ and fitted again the delays vs cycles. Δ_{tot} are the errors associated to the dip arrival times shown in Tab. 1.

We obtained six dip arrival times one from Chandra, two from the folded MAXI light curves, and, finally, three from the folded RXTE/ASM light curves. We corrected the orbital period fitting the delays with a linear function. The linear ephemeris is

$$T_{dip} = 50,086.72(7)\ \mathrm{MJD} + 24.5277(3)N, \quad (1)$$

where N is the number of cycles, 50, 086.72(7) is the new Epoch of reference, and the revised orbital period is $P = 24.5277(3)$ d. The χ^2(d.o.f.) is 5.8(4) and the associated errors are at 68% confidence level. Here and in the following the uncertainties in the parameters have been scaled by a factor $\sqrt{\chi^2_{red}}$ to take into account a χ^2_{red} of the best-fit model larger than 1. We show the delays versus the orbital cycles, together with the best-fit linear ephemeris, in Fig. 15 (left panel).

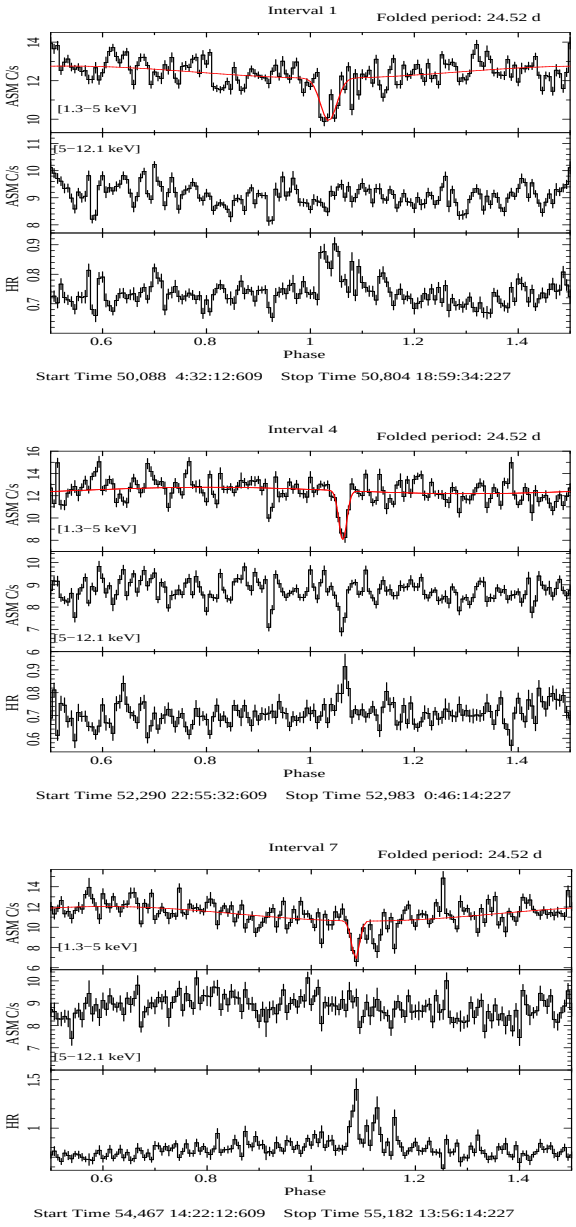

Fig. 13. ASM folded light curves of GX 13+1 in the 1.3-5 keV (top panels) and 5-12.1 keV energy band (middle panels) covering about 714 days. The corresponding hardness ratios are plotted in the bottom panels. The folding period is 24.52 d and 150 phase-bins per period were adopted. The red solid line is the best-fit curve composed of a constant plus a sinusoidal function with period kept fixed to 24.52 d and a Gaussian profile fitting the dip.

We also determined the linear ephemeris excluding the Chandra point to avoid the possibility that our result is driven by it. In this case we found that the new epoch of reference is 50, 086.73(9) and the revised orbital period is $P = 24.5276(5)$ d. This result is compatible, within 1 σ, with that shown in Eq. 1 and suggests that the Chandra point does not drive the fit and that the dip observed in the Chandra light curve is periodic. Furthermore, we started with a trial period of 24.52 d obtain-

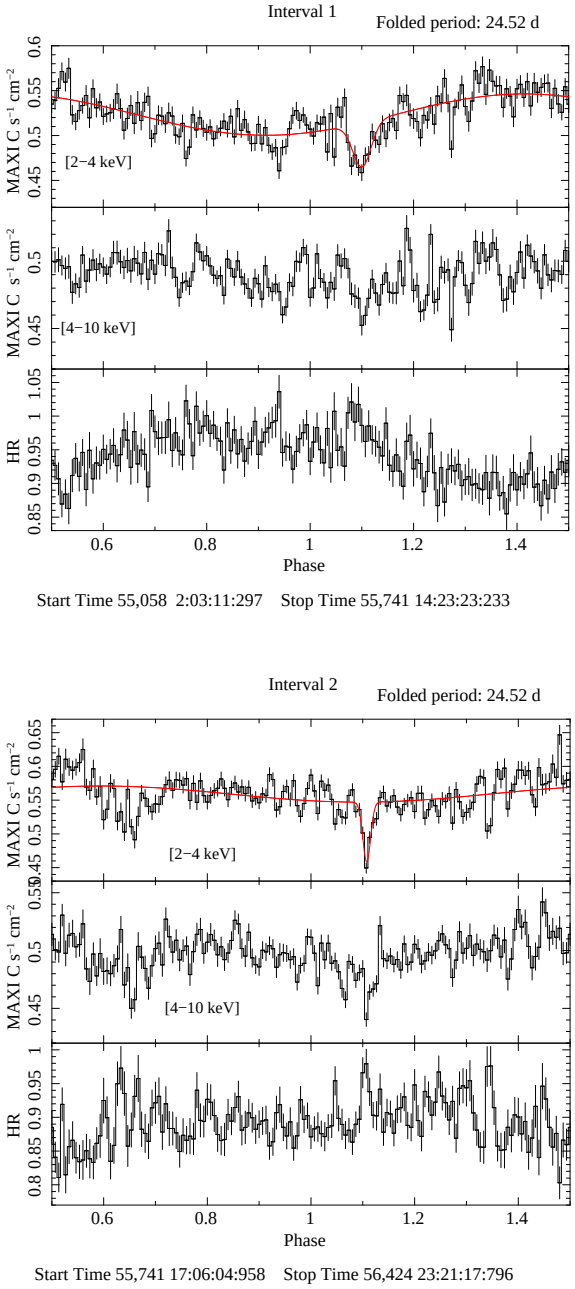

Fig. 14. MAXI folded light curves of GX 13+1 in the 2-4 keV (top panels) and 4-10 keV energy band (middle panels) covering about 680 days. The folding period is 24.52 d and 150 phase-bins per period were adopted. The red solid line is defined in the text and Fig. 13.

ing, finally, a period of 24.5277 d that is very similar to the value of 24.53 d obtained independently searching for periodicities in the ASM and MAXI light curves (see Figs. 4 and 5).

Then, we applied again the whole procedure to the ASM and MAXI light curves adopting as folding period 24.5277 d and as epoch of reference 50,086.72 MJD to refine our results. The selected intervals for the two light curves are the same described above. Using these two accurate values we were able to detect a periodic dip also in the interval 2 of the ASM light curves. The journal of the seven dips is shown in Tab. 2.

We corrected the orbital period fitting the seven delays with a linear function. The linear fit of the seven points is shown in Fig. 15 (right panel). The refined linear ephemeris is

$$T_{dip} = 50,086.79(3)\ \mathrm{MJD} + 24.5274(2)N. \quad (2)$$

The χ^2(d.o.f.) is 6.76(5) and the associated errors are at 68% confidence level. We folded the 1.3-5 keV and 5-12.1 keV ASM light curves adopting the epoch of references and the period of Eq. 2 (Fig. 16; left panels), both the light curves cover ∼ 236 cycles. The periodic dip is evident in both the ASM energy bands and the HR shows at zero phase a more pronounced increasing. To quantify the improvement of the orbital period after the correction achieved using the timing technique we defined the fraction $f = (HR_{max} - HR_{ave})/(HR_{max} + HR_{ave})$, where HR_{ave} is the average value of HR between phase 0.1 and 0.9 and HR_{max} is the HR at phase 0. We obtain that f is 6.1% and 8.6% in the HR obtained folding the ASM light curves with a period of 24.53 and 24.5274 d, respectively.

We folded the 2-4 keV and 4-10 keV MAXI light curves adopting the epoch of references and the period of Eq. 2 (Fig. 16, right panels), both the light curves covers ∼ 56 cycles. The value of f is 4.5% and 5% in the HR obtained folding the MAXI light curves with a period of 24.53 and 24.5274 d, respectively. The largest increase of the HR associated with the ASM light curves is mainly due to the wider spanning time that ASM covers (∼ 16 yr) with respect to MAXI (∼ 4 yr).

Finally, we added a quadratic term to the ephemeris to take into account a possible period derivative. In this case, we obtained the following quadratic ephemeris

$$T_{dip} = 50,086.80(7)\ \mathrm{MJD} + 24.5271(13)N + 9(46)\times10^{-7}N^2, \quad (3)$$

with a χ^2(d.o.f.) of 6.7(4). Adding the quadratic term we do not obtain a significant improvement of the fit. The corresponding period derivative is $8(37)\times10^{-8}$ s/s with the associated error at 68% confidence level. The best-fit curve associated to the quadratic ephemeris is shown in Fig. 15 (right panel) with a dashed curve.

Using the linear ephemeris of Eq. 2 we determined the expected dip arrival time nearest the RGS observation discussed in section 2.4. The corresponding cycle number is 182 and the predicted arrival time is 54,550.78 MJD. In Fig. 12 we show the RXTE/ASM light curve between 54,545 and 54,555 MJD. We indicate the start and stop times (54,550.97 and 54,551.12 MJD, respectively) of the RGS observation with the red-dashed vertical lines; the predicted dip arrival time using the ephemeris of Eq. 2 is plotted with a red-solid vertical line. The separation in units of orbital phase of the expected dip arrival time from the RGS start time is only 0.19 d. We conclude that our predicted arrival time is compatible with the ASM light curve and that the RGS instruments observed only the final part of a periodic dip.

Díaz Trigo et al. (2012) suggested the presence of possible dipping states in RXTE/PCA, EXOSAT, ans XMM observations. We, therefore, searched for possible periodic dips in the RXTE/PCA archival data. We analysed the barycentred 2-4 and 4-9 keV light curves obtained from the standard 2 products finding that there are no observations covering the phase zero (i.e. the phase at which we expect the dip), except for observation P95338-01 that unfortunately has a hole in the light curve at the expected dip arrival time (see sec. 2.1). The observation P95338-01 spans 12 days covering almost one half of the orbital period. The hardness ratio ranges between 2 and 2.6, reaching the maximum value at phases 0.95 and close to 1.

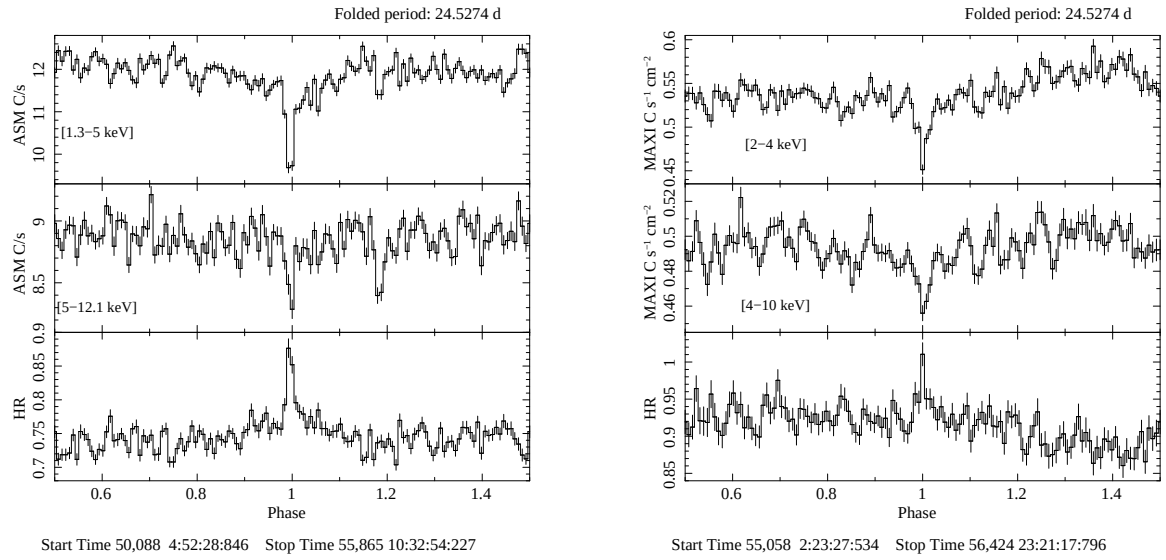

Fig. 16. RXTE/ASM (left panel) and MAXI (right panel) folded light curves and the corresponding hardness ratios using the ephemeris of Eq. 1. The RXTE and MAXI light curves are folded using 128 phase-bins per period.

Table 3. Journal of the XMM observations of GX 13+1

Obs. Num.	Observation ID	Start Time (UTC) year month day	hr:min	Orbital Phase	Dipping State
1	0122340101	2000 March 30	14:10	0.06	deep
2	0122340901	2000 April 01	4:29	0.13	shallow
3	0122341001	2000 April 01	8:51	0.14	deep
4	0505480101	2008 March 09	15:48	0.34	shallow
5	0505480701	2008 March 11	19:00	0.43	–
6	0505480201	2008 March 11	23:10	0.44	persistent
7	0505480301	2008 March 22	02:20	0.85	shallow
8	0505480501	2008 March 25	23:01	0.007	deep
9	0505480401	2008 September 5	21:49	0.69	deep

Note — The phase is associated to the start time of the observation and it is calculated using the ephemeris of Eq. 2. The dipping state shown in the sixth column is discussed by Díaz Trigo et al. (2012). For the observation 5 only RGS and the optical monitor (OM) were available.

Díaz Trigo et al. (2012) suggested a possible dipping state of GX 13+1 observed with the RXTE/PCA in the observations P30050-01 and P30051-01. However, the authors did not perform a systematic search for dips and their suggestion is based on the bi-modal behaviour of the count rate with the hardness ratio reported by Schnerr et al. (2003). We reanalysed the RXTE/PCA observations P30050-01 and P30051-01 which span a time interval from 50,950 to 51,096 MJD (i.e. 5.94 orbital cycles for a period of 25.5274 d). We analysed the barycentred 2-4 and 4-9 keV light curves and extracted the corresponding HR. We found that the HR has an erratic behaviour along the orbital phase varying between 2.5 and 3.5 and reaching the maximum value of 3.8 at phase 0.38. The observations do not cover the phase at which the periodic dip is expected; the pointed observations closest to the zero-phase are P30051-01-06-00 and P30051-01-10-00 (phase at the start time 0.98 and 0.97, respectively). Finally, we also analysed the RXTE/PCA observations P40023-03 and P40022-01 which span ∼ 171 days (i.e. ∼ 7 orbital periods). The HR ranges between 1.8 and 2.2 and has a peak at phase 0.19 reaching the value of 2.7.

Díaz Trigo et al. (2012) also suggested the presence of a possible dipping state of GX 13+1 in the EXOSAT observation taken on 1983 Sep. 22 (see sec. 2.1); using the linear ephemeris of eq. 2 we find that the start time of that observation corresponds at phase 0.07 meaning that the dip arrival time is predicted at ∼ 144 ks before the start time), that is quite far from the expected periodic dip arrival time. The EXOSAT observation taken on 1985 May 2 corresponds to an orbital-phase interval 0.015-0.029, that is ∼33 ks after the expected periodic dip.

The presence of dipping states was also suggested in XMM/Epic-pn observations. For sake of completeness we report in Tab. 3 the list of the XMM observations of GX 13+1 using the same indices adopted by Díaz Trigo et al. (2012) in their paper. We added as further information the orbital phase associated to each of the XMM/Epic-pn start time adopting the ephemeris of eq. 2. In this case we converted in phase the start time in UTC instead of TDB; however, in our case, the effects of the barycentre correction is irrelevant because of the large period of 24.5274 d. We note that the dipping states of GX 13+1 suggested by Díaz Trigo et al. (2012) are almost independent on the orbital phase.

Finally, Chandra observed GX 13+1 nine times; we report in Tab. 4 the list of the observations and the orbital phase at the start time of each Chandra observation.

Table 4. Journal of the Chandra observations of GX 13+1

Observation	Start Time (UTC)		Orbital Phase
ID	year month day	hr:min:sec	
950	2000 August 7	00:00:05	0.34
2708	2002 October 8	11:12:56	0.65
6093	2005 February 8	19:50:44	0.48
11815	2010 July 24	05:46:27	0.67
11816	2010 July 30	14:47:25	0.93
11814	2010 August 1	00:31:31	0.99
11817	2010 August 3	10:12:10	0.09
11818	2010 August 5	14:09:39	0.18
13197	2011 February 17	17:57:04	0.18

NOTE — The phase is associated to the start time of the observation and it is calculated using the ephemeris of Eq. 2. The observation id. 11814 is discussed in sec. 2.1.

4. Discussion and Conclusion

In this paper we have analysed archival data of GX 13+1 from Chandra, XMM, RXTE, EXOSAT, and MAXI, with the aim to look for periodic dips in this source. Using a Chandra/HETG observation we improved the X-ray position of GX 13+1, that is now compatible with the positions of the infrared and radio counterparts of GX 13+1. Using the new coordinates we barycentred the ASM and MAXI light curve of GX 13+1. We performed a PSD of the 1.3-12.1 keV ASM light curve detecting a periodic signal at a period between 22.78 and 26.92 d. To refine the periodic signal we used the ftool *efsearch* and looked at the period-window between 22.78 and 26.92 d in the 1.3-12.1 keV ASM and 2-10 keV MAXI light curves. We detected a significant common periodic signal in the two light curves at 24.53 d. The 24.53 d folded ASM and MAXI light curves in two different energy bands (1.3-5 and 5-12.1 keV for ASM and 2-4 and 4-10 keV for MAXI) and the corresponding HRs clearly show that the periodic signal is associated to a periodic dip present in the light curves.

To improve the value of 24.53 d and to obtain the orbital ephemeris of GX 13+1 we used the timing technique dividing the ASM and MAXI light curves in eight and two time intervals, respectively. Finally we obtained four dip arrival times from the ASM light curves and two dips arrival times from the MAXI light curve. We showed that the dip observed in a recent Chandra observation is well fitted using the ephemeris obtained by our dip arrival times. The linear ephemeris gave a refined period of 24.5274(2) d that we interpret as the orbital period of the system.

So far, the absence of periodic signatures in the light curve of GX 13+1 has made difficult an accurate estimation of its orbital period. Before this work, the most accurate estimation of the orbital period of the system was given by Corbet et al. (2010), who looked for periodicities in the RXTE/ASM light curve spanning 14 years, finding a period of 24.27 ± 0.03 days that is not compatible with our result; however, the associated error to the period reported by Corbet et al. (2010) is a formal statistical error and it could be larger. The detection of periodic dips allows us to determine accurate X-ray ephemeris of GX 13+1 and improve the accuracy of the period by a factor one hundred.

From the analysis of the delays associated with the dip arrival times we obtained the linear and quadratic ephemerides of GX 13+1. The goodness of our orbital solution is evident when we fold the whole RXTE/ASM and MAXI light curves (Fig. 16) after correcting the event arrival times for the new orbital solution, since in this case both the light curves show a clear dip at zero phase with a corresponding increase of the HRs. If the proposed period of 24.5274 d, obtained by studying the periodic dips in the light curve of GX 13+1, will be confirmed as the orbital period of the system, then GX 13+1 has the longest known orbital period for a Galactic LMXB hosting a neutron star and powered by Roche lobe overflow.

A posteriori we searched for periodic dips in all pointed observations of GX 13+1. Díaz Trigo et al. (2012) suggested the presence of possible dipping states in EXOSAT (see Stella, White & Taylor 1985), RXTE/PCA (see Schnerr et al. 2003), and XMM/Epic-pn observations (see Díaz Trigo et al. 2012). We have analysed these observations finding that these dipping states are not related with the orbital phase. We believe that the periodic dips shown in this work are connected to the periodic motion of the hot spot at the outer accretion disc caused by the impact of the stream of matter from the companion star. On the other hand, the dipping state in GX 13+1 observed by Díaz Trigo et al. (2012) in some XMM observations and the bi-modal behaviour of the hardness ratio with respect to the intensity of the source observed by Schnerr et al. (2003) in the RXTE/PCA observations P30050-01 and P30051-01 and by Stella, White & Taylor (1985) in the EXOSAT observation taken on 1983 September 22, may be caused by partial absorption in the large outflow of matter from the inner region of the system detected by several authors (see e.g. Ueda et al. 2001, 2004; Díaz Trigo et al. 2012).

Finally, we also tried to estimate the orbital period derivative and we reported the quadratic ephemeris of the source. We find only a loose constraint on the period derivative of $8(37) \times 10^{-8}$ s/s, with the error at 68% confidence level. The large associated uncertainty to the quadratic term does not allow us to draw a firm conclusion, and further observations are needed to constrain this result.

Acknowledgements

This research has made use of MAXI data provided by RIKEN, JAXA and the MAXI team. AR Gratefully acknowledges Sardinia Regional Government for the financial support (P.O.R. Sardegna F.S.E. Operational Programme of the Autonomous Region of Sardinia, European Social Fund 2007-2013 - Axis IV Human Resources, Objective l.3, Line of Activity l.3.1 Avviso di chiamata per il finanziamento di Assegni di Ricerca). Work in Cagliari was partially funded by the Regione Autonoma della Sardegna through POR-FSE Sardegna 2007-2013, L.R. 7/2007, Progetti di ricerca di base e orientata, Project N CRP-60529

References

Bandyopadhyay R. M., Shahbaz T., Charles P. A., Naylor T., 1999, MNRAS, 306, 417
Corbet R. H. D., 2003, ApJ, 595, 1086
Corbet R. H. D., Pearlman A. B., Buxton M., Levine A. M., 2010, ApJ, 719, 979
Díaz Trigo M., Sidoli L., Boirin L., Parmar A. N., 2012, A&A, 543, A50
Fleischman J. R., 1985, A&A, 153, 106
Garcia M. R., Grindlay J. E., Bailyn C. D., Pipher J. L., Shure M. A., Woodward C. E., 1992, AJ, 103, 1325
Grindlay J. E., Seaquist E. R., 1986, ApJ, 310, 172
Iaria R., Di Salvo T., Burderi L., D'Aí A., Papitto A., Riggio A., Robba N. R., 2011, A&A, 534, A85
Iaria R., di Salvo T., Lavagetto G., D'Aí A., Robba N. R., 2007, A&A, 464, 291
Iaria R., Di Salvo T., Lavagetto G., Robba N. R., Burderi L., 2006, ApJ, 647, 1341
Matsuba E., Dotani T., Mitsuda K., Asai K., Lewin W. H. G., van Paradijs J., van der Klis M., 1995, PASJ, 47, 575
Matsuoka M. et al., 2009, PASJ, 61, 999
Schnerr R. S., Reerink T., van der Klis M., Homan J., Méndez M., Fender R. P., Kuulkers E., 2003, A&A, 406, 221

Sidoli L., Parmar A. N., Oosterbroek T., Lumb D., 2002, A&A, 385, 940
Smith R. K., 2008, ApJ, 681, 343
Smith R. K., Edgar R. J., Shafer R. A., 2002, ApJ, 581, 562
Stella L., White N. E., Taylor B. G., 1985, in ESA Special Publication, Vol. 236, Recent Results on Cataclysmic Variables. The Importance of IUE and Exosat Results on Cataclysmic Variables and Low-Mass X-Ray Binaries, Burke W. R., ed., pp. 125–128
Ueda Y., Asai K., Yamaoka K., Dotani T., Inoue H., 2001, ApJ, 556, L87
Ueda Y., Murakami H., Yamaoka K., Dotani T., Ebisawa K., 2004, ApJ, 609, 325